On the Aromaticity and Meisenheimer Rearrangement of Strained Heterocyclic Amine, Phosphine, and Arsine Oxides

José Molina Molina,† Redouan El-Bergmi, J. A. Dobado,* and Dolores Portal

Grupo de Modelización y Diseño Molecular, Instituto de Biotecnología, Campus Fuentenueva s/n, Universidad de Granada, 18071-Granada, Spain

dobado@ugr.es

Received August 11, 2000

A theoretical investigation (AIM and ELF analyses together with NMR chemical shifts) has been conducted for three-membered heterocycle (N, P, and As) oxides. An aromatic stabilization was found for the P and As rings. However, the N derivatives displayed a net negative hyperconjugation in the N−O bond formation, without ring aromaticity observed for their electronic properties. The calculated δ_C and δ_H shifts also supported the ring delocalization for the P and As unsaturated heterocycle oxides ($\delta_C \approx 165$ and $\delta_H \approx 9$ ppm). In addition, these values for 1*H*-azirine oxide resembled standard C=C double bond values ($\delta_C \approx 130$ and $\delta_H \approx 7$ ppm). The different behavior for the N oxides was also observed in their Meisenheimer rearrangement (MR). All the reaction paths, yielding the corresponding hydroxyl structures, were exothermic (G2 method). However, the N derivatives showed the lowest values for activation enthalpy, $\Delta H^{\ddagger}$. The C=C bond influence in the MR was slight, with the same ΔH values for the saturated and unsaturated paths. This rearrangement for the P and As oxides yielded TSs closer to the reactives; however, the corresponding TSs resembled the products for the N-derivatives. The different reaction paths have been examined by their corresponding AIM and ELF analyses at the B3LYP/6-311G* level.

I. Introduction

The bond nature for phosphine oxides and related compounds has been controversial for years.[1] In this context, it has been demonstrated that the *d* orbitals do not participate in the P−O bond.[2] The nature of this bond has been explained in terms of a combination of two different resonance forms

$$R_3P^+-O^- \leftrightarrow R_3P=O \qquad (1)$$

following three alternatives: (a) the negative hyperconjugation of Reed and Schleyer[3] (one σ and two π-back-bonds), (b) the view of Streitwieser[4] and Schmidt[5] (one σ and three π-back-bonds), and (c) the banana bond scheme (three Ω-bonds).[5−8] These possibilities arose from different analyses of the theoretical wave function. In this sense, Cioslowski pointed out the necessity of analyzing the computed wave function in a rigorous manner by employing definitions that are fully independent of the methods used in calculation or the wave function and the characters of the molecules analyzed.[9] Thus, in the interpretation and analysis of the electronic wave function, only observable-based theoretical tools should be applied.[10]

The atoms in molecules theory (AIM)[11,12] has shown its utility in describing this bond as *a polar single σ bond which has characteristics determined mainly by electrostatic interactions*.[13]

Among the topological analyses of the electron charge density, $\rho(r)$, a complementary viewpoint in the AIM theory arises from the analysis of the electron localization function (ELF).[14−17]

The electronic structure of the three-membered phosphirene ring has been a matter of debate concerning its possible antiaromatic character,[18−21] and several theoretical descriptions have been applied to phosphirenes and derivatives,[22−24] including the topological analysis of the $\rho(r)$.[20]

Phosphirene has been described[19] as a nonantiaromatic system, due mainly to the nonplanarity of the structure.

* To whom correspondence should be addressed. Tel/Fax: +34-958-243186.

† Professor José Molina Molina passed away on 13 June 2000.

(1) For an extensive review, see: Gilheany, D. G. *Chem. Rev.* **1994**, *94*, 1339 and references therein.
(2) For a detailed discussion on the noninvolvement of the *d* orbitals, see ref 1.
(3) Reed, A. E.; Schleyer, P. v. R. *J. Am. Chem. Soc.* **1990**, *112*, 1434.
(4) Streitwieser, A.; Rajca, A.; McDowell, R. S.; Glaser, R. *J. Am. Chem. Soc.* **1987**, *109*, 4184.
(5) Schmidt, M. W.; Yabushita, S.; Gordon, M. S. *J. Phys. Chem.* **1984**, *88*, 382.
(6) Guest, M. F.; Hillier, I. H.; Saunders, V. R. *J. Chem. Soc., Faraday Trans. 2* **1972**, 867.
(7) Molina, P.; Alajarín, M.; Leonardo, C. L.; Claramunt, R. M.; Foces-Foces, M. D. L. C.; Cano, F. H.; Catalán, J.; de Paz, J. L. G.; Elguero, J. *J. Am. Chem. Soc.* **1989**, *111*, 355.
(8) Schultz, P. A.; Messmer, R. P. *J. Am. Chem. Soc.* **1993**, *115*, 10938.
(9) Cioslowski, J.; Mixon, S. T. *Inorg. Chem.* **1993**, *32*, 3209.
(10) Cioslowski, J.; Surjan, P. R. *THEOCHEM* **1992**, *255*, 9.
(11) Bader, R. F. W. *Atoms in Molecules: a Quantum Theory*; Clarendon Press: Oxford, 1990.
(12) Bader, R. F. W. *Chem. Rev.* **1991**, *91*, 893.
(13) Dobado, J. A.; Martínez-García, H.; Molina, J.; Sundberg, M. R. *J. Am. Chem. Soc.* **1998**, *120*, 8461.
(14) Becke, A. D.; Edgecombe, K. E. *J. Chem. Phys.* **1990**, *92*, 5397.
(15) Silvi, B.; Savin, A. *Nature* **1994**, *371*, 683.
(16) Savin, A.; Nesper, R.; Wengert, S.; Fässler, T. F. *Angew. Chem., Int. Ed. Engl.* **1997**, *36*, 1809.
(17) Marx, D.; Savin, A. *Angew. Chem., Int. Ed. Engl.* **1997**, *36*, 2077.
(18) Marinetti, A.; Mathey, F.; Fischer, J.; Mitschler, A. *J. Chem. Soc., Chem. Commun.* **1984**, *45*.
(19) Bachrach, S. M. *J. Org. Chem.* **1991**, *56*, 2205.
(20) Bachrach, S. M. *THEOCHEM* **1992**, *255*, 207.
(21) Nguyen, M. T.; Vansweevelt, H.; Vanquickenborne, L. G. *Chem. Ber.* **1992**, *125*, 923.

10.1021/jo0056040 CCC: $19.00
Published on Web 11/17/2000

Scheme 1. Meisenheimer Rearrangement (MR) Reaction Paths of the Saturated and Unsaturated rings, for N, P, and As Derivatives, at the B3LYP/6-311G* Level (All in kcal·mol^{-1})

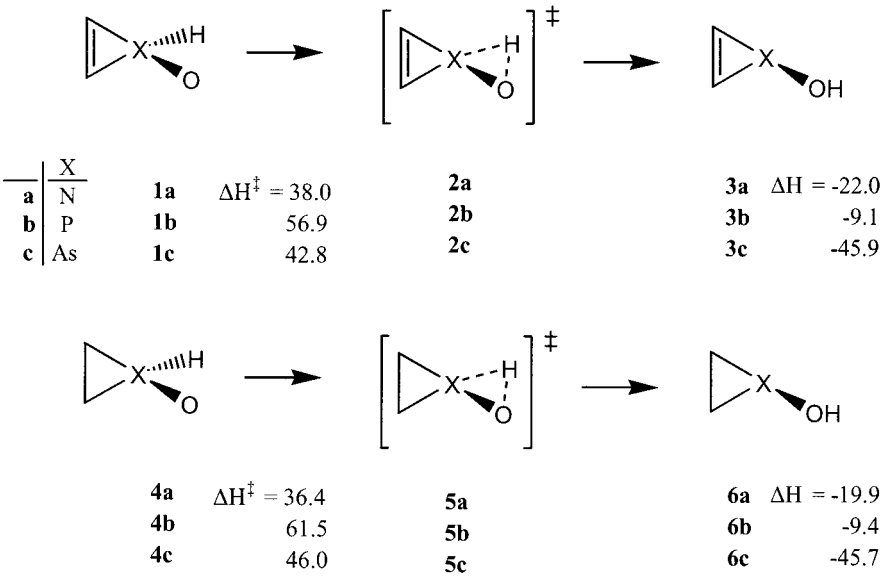

On the other hand, the phosphirenylium cations present aromaticity.

The highly ionic character of the phosphine oxide P−O bond implies two π electrons in the ring and can be considered to be an aromatic system.

The Meisenheimer rearrangement (MR) has been described, in tertiary amine oxides on heating, to give substituted hydroxylamines.[25,26]

$$R_3N-O \rightarrow R_2N-OR \qquad (2)$$

Recently, the MR has been widely used in organic synthesis.[27−31] However, no previous theoretical studies on this rearrangement are available in the literature.

The MR is related to that of Stevens (SR), originally discovered in nitrogen ylides,[32] and it has also been shown to take place in sulfur ylides.[33−35] This reaction occurs thermally to give amines and sulfides derivatives. The mechanism of SR, which has long been a topic of discussion for years,[36,37] has been understood considering such experimental facts as stereospecifity[38,39] and intramolecularity.[40,41] Very recently, theoretical studies on SR have been reported for amine, phosphine, and arsine ylides[42,43] and related rearrangements of imino phosphoranes and iminoarsoranes.[44] Moreover, a comparison has been performed between a concerted migration and a radical dissociation−recombination path. In both MR and SR, an alternative [2,3]-migration has also been postulated.[43,45]

The goal of the present work is to characterize the influence of the P−O and C=C bonds in the aromaticity and in the MR, for phosphirene and their saturated phosphorane P-oxide heterocycles. In this effort, a comparative investigation (AIM and ELF analyses together with calculated chemical shifts) for the nitrogen and arsenic series of compounds is also included (see Scheme 1).

II. Computational Details

A. General Methods. Density functional theory (B3LYP) calculations were performed with the Gaussian 98 package of programs.[46] All the minimum structures were fully optimized and tested by frequency analysis at the B3LYP/6-311G* level, yielding the minima with constrained (C_s) symmetry non-

(22) Göller, A.; Clark, T. *Chem. Commun.* **1997**, 1033.
(23) Lee, E. P. F.; Nyulászi, L.; Veszprémi, T. *J. Phys. Chem.* **1994**, *98*, 6481.
(24) Eisfeld, W.; Regitz, M. *J. Org. Chem.* **1998**, *63*, 2814.
(25) Meisenheimer, J. *Ber. Dtsch. Chem. Ges.* **1919**, *42*, 1667.
(26) For a review of Meisenheimer rearrangement in synthesis see: Albini, A. *Synthesis-Stuttgart* **1993**, 263.
(27) Davies, S. G.; Smyth, G. D. *J. Chem. Soc., Perkin Trans. 1* **1996**, 2467.
(28) Fulop, F.; Bernath, G. *Current Org. Chem.* **1999**, *3*, 1.
(29) Buston, J. E. H.; Coldham, I.; Mulholland, K. R. *J. Chem. Soc. Perk. Trans. 1* **1999**, 2327.
(30) Majumdar, K. C.; Jana, G. H. *J. Org. Chem.* **1997**, *62*, 1506.
(31) Arnone, A.; Metrangolo, P.; Novo, B.; Resnati, G. *Tetrahedron* **1998**, *54*, 7831.
(32) Stevens, T. S.; Creighton, E. M.; Gordon, A. B.; MacNicol, M. *J. Chem. Soc.* **1928**, 3193.
(33) Blackburn, G. M.; Ollis, W. D.; Plackett, J. D.; Smith, C.; Sutherland, I. O. *Chem. Commun.* **1968**, 186.
(34) Baldwin, J. E.; Hackler, R. E.; Kelly, D. P. *Chem. Commun.* **1968**, 1083.
(35) Baldwin, J. E.; Hackler, R. E. *J. Am. Chem. Soc.* **1969**, *91*, 3646.
(36) Stevens, T. S.; Watts, W. E. *Selected Molecular Rearrangements*; van Nostrand Reinhold: London, 1973; p 81.
(37) Pine, S. H. *Org. React.* **1970**, *18*, 403.
(38) Millard, B. J.; Stevens, T. S. *J. Chem. Soc.* **1963**, 33.
(39) Scholkkopf, U.; Ludwig, U.; Ostermann, G.; Patsch, M. *Tetrahedron Lett.* **1969**, 3415.
(40) Ollis, W. D.; Rey, M.; Sutherland, I. O. *J. Chem. Soc., Perkin Trans. 1* **1983**, 1009.
(41) Johnstone, R. A. W.; Stevens, T. S. *J. Chem. Soc.* **1955**, 4487.
(42) Makita, K.; Koketsu, J.; Ando, F.; Ninomiya, Y.; Koga, N. *J. Am. Chem. Soc.* **1998**, *120*, 5764.
(43) Heard, G, L.; Yates, B. F. *J. Org. Chem.* **1996**, *61*, 7276.
(44) Makita, K.; Koketsu, J.; Ninomiya, Y.; Koga, N. *Nippon Kagaku Kaishi* **1999**, 397.
(45) Craig, J. C.; Ekwuribe, N. N.; Gruenke, L. D. *Tetrahedron Lett.* **1979**, 4025.
(46) Gaussian 98, revision A.7. Frisch, M. J.; Trucks, G. W.; Schlegel, H. B.; Scuseria, G. E.; Robb, M. A.; Cheeseman, J. R.; Zakrzewski, V. G.; Montgomery, J. A., Jr.; Stratmann, R. E.; Burant, J. C.; Dapprich, S.; Millam, J. M.; Daniels, A. D.; Kudin, K. N.; Strain, M. C.; Farkas, O.; Tomasi, J.; Barone, V.; Cossi, M.; Cammi, R.; Mennucci, B.; Pomelli, C.; Adamo, C.; Clifford, S.; Ochterski, J.; Petersson, G. A.; Ayala, P. Y.; Cui, Q.; Morokuma, K.; Malick, D. K.; Rabuck, A. D.; Raghavachari, K.; Foresman, J. B.; Cioslowski, J.; Ortiz, J. V.; Stefanov, B. B.; Liu, G.; Liashenko, A.; Piskorz, P.; Komaromi, I.; Gomperts, R.; Martin, R. L.; Fox, D. J.; Keith, T.; Al-Laham, M. A.; Peng, C. Y.; Nanayakkara, A.; Gonzalez, C.; Challacombe, M.; Gill, P. M. W.; Johnson, B. G.; Chen, W.; Wong, M. W.; Andres, J. L.; Head-Gordon, M.; Replogle, E. S.; Pople, J. A. *Gaussian 98*, revision A.7; Gaussian, Inc.: Pittsburgh, PA, 1998.

imaginary frequencies, and only one imaginary frequency for the transition states (TSs) without symmetry restrictions. The isodesmic reactions have been accurately estimated at the G2 level[47] within the Gaussian 98 program.[46]

The AIM analysis[11,12] has been performed with the AIMPAC series of programs,[48] using the DFT densities as the input.

The NMR chemical shifts were calculated by the GIAO method[49] using the tetramethylsilane (TMS) shieldings as references for the ^{1}H (δ_H) and ^{13}C (δ_C) chemical shifts.

The $\nabla^2\rho$(r) contour-map representations have been produced using the MORPHY98 program.[50] The ELF analyses have been made with the TopMoD package of programs.[51]

B. Overview of the $\rho(r)$ and ELF Topologies. The topology of the electronic charge density, $\rho(r)$, as pointed out by Bader,[11] is an accurate mapping of the chemical concepts of atoms, bonds, and structures. The principal topological properties are summarized in terms of their critical points (CP),[11,12] and the nuclear positions behave topologically as local maxima in $\rho(r)$. A bond critical point (BCP) is found between each pair of nuclei, which are considered to be linked by a chemical bond, with two negative curvatures, (λ_1 and λ_2) and one positive (λ_3) (denoted as (3,−1) CP). The ellipticity, ϵ, of a bond is defined by means of the two negative curvatures in a BCP as

$$\epsilon = \lambda_1/\lambda_2 - 1$$

where

$$|\lambda_2| < |\lambda_1| \tag{3}$$

The ring CPs are characterized by a single negative curvature. Each (3,−1) CP generates a pair of gradient paths[11] that originate at a CP and terminate at neighboring attractors. This gradient path defines a line through the charge distribution linking the neighboring nuclei. Along this line, ρ(r) is a maximum with respect to any neighboring line. Such a line is referred to as an atomic interaction line.[11,12] The presence of an atomic interaction line in such equilibrium geometry satisfies both the necessary and sufficient conditions that the atoms be bonded together.

The Laplacian of the electronic charge density, $\nabla^2\rho(r)$, describes two extreme situations. In the first, $\rho(r)$ is locally concentrated ($\nabla^2\rho(r) < 0$), and in the second, it is locally depleted ($\nabla^2\rho(r) > 0$). Thus, a value of $\nabla^2\rho(r) < 0$ at a BCP is unambiguously related to a covalent bond, showing that a sharing of charge has taken place. While in a closed-shell interaction, a value of $\nabla^2\rho(r) > 0$ is expected, as found in noble gas repulsive states, ionic bonds, hydrogen bonds, and van der Waals molecules. Bader has also defined a local electronic energy density, $E_d(r)$, as a functional of the first-order density matrix

$$E_d(r) = G(r) + V(r) \tag{4}$$

where the $G(r)$ and $V(r)$ correspond to a local kinetic and potential energy density, respectively.[11] The sign of the $E_d(r)$ determines whether a charge accumulation at a given point r is stabilizing ($E_d(r) < 0$) or destabilizing ($E_d(r) > 0$). Thus, a value of $E_d(r) < 0$ at a BCP presents a significant covalent contribution and, therefore, a lowering of the potential energy associated with the concentration of charge between the nuclei.

The ELF function,[14−17] which was first introduced by Becke and Edgecombe,[14] can be viewed as a local measure of the Pauli repulsion between electrons due to the exclusion principle, enabling us to define regions of space that are associated with different electron pairs. The ELF function is expressed by

$$\mathrm{ELF} = \frac{1}{1 + \left(\frac{D}{D_h}\right)^2} \tag{5}$$

where

$$D = \frac{1}{2}\sum_{j=1}^{N}\left|\nabla\varphi_j\right|^2 - \frac{1}{8}\frac{|\nabla\rho|^2}{\rho};\ D_h = \frac{3}{10}(3\pi^2)^{2/3}\rho^{5/3};\ \rho = \sum_{j=1}^{N}\left|\varphi_j\right|^2 \tag{6}$$

This definition gives ELF values between 0 and 1, with large values where two antiparallel spin electrons are paired in space; on the contrary, this value is small in the regions between electron pairs.

III. Results and Discussion

The MR is studied on amine, phosphine, and arsine three-membered ring derivatives. Moreover, the saturated and unsaturated rings are compared in order to demonstrate the participation of the double bond in the reaction (see Scheme 1). As pointed out in the Introduction, there are possible competing mechanisms in this rearrangement, including the [1,2]-shift concerted one, the radical path, as well as the competing [2,3]-rearrangement. Therefore, the theoretical study of the MR was started with the [1,2]-shift hydrogen migration concerted path to yield the hydroxyl derivatives.

In Scheme 1, the rearrangement paths are illustrated, including the activation enthalpy, $\Delta H^{\ddagger}$, for the TSs (**2a**−**c** and **5a**−**c**) and the relative enthalpy, ΔH, of the corresponding hydroxyl derivatives (**3a**−**c** and **6a**−**c**), compared to the corresponding oxides (**1a**−**c** and **4a**−**c**). All the reactions, yielding amine-, phosphine- or arsine-hydroxyl derivatives, were exothermic by 20−22 kcal·mol^{-1} for N, 9 kcal·mol^{-1} for P, and 45 kcal·mol^{-1} for As, respectively. The corresponding $\Delta H^{\ddagger}$ values for the concerted [1,2]-shift are high enough (36−61 kcal·mol^{-1}) in agreement with the Woodward−Hoffmann[52] rule for the forbidden suprafacial migration. The influence of the C═C double bond in the above-mentioned reactions is not remarkable, the differences in $\Delta H^{\ddagger}$ values between the unsaturated and saturated rings were small (2−4 kcal·mol^{-1}), yielding a decrease in N and an increase in P or As compounds. The variation of ΔH for the different hydroxyl pathways (<0.3 for P or As and 2.1 kcal·mol^{-1} for N derivatives) was also minor.

As mentioned in the Introduction, the radical path was postulated as a reasonable alternative for the SR.[43,45] To test this alternative, we calculated the radical P−H homolitic breaking of **1b**, and found the energy of this reaction to be 82.6 kcal·mol^{-1}, higher by 25 kcal·mol^{-1} than the corresponding $\Delta H^{\ddagger}$ of the concerted [1,2]-shift. Consequently, this radical dissociation−recombination pathway was discarded.

An aromatic-like stabilization for the unsaturated structures (**1a**−**c**) can be explained by the electron-withdrawing effects of the coordinated oxygen. A set of isodesmic reactions have been performed to test this stabilization (see Scheme 2). Furthermore, for the As derivatives the saturated isodesmic reaction ii were

(47) Curtiss, L. A.; Raghavachari, K.; Trucks, G. W.; Pople, J. A. *J. Chem. Phys.* **1991**, *94*, 7221.

(48) Biegler-König, F. W.; Bader, R. F. W.; Tang, T.-H. *J. Comput. Chem.* **1982**, *3*, 317.

(49) Wolinski, K.; Hilton, J. F.; Pulay, P. *J. Am. Chem. Soc.* **1990**, *112*, 8251.

(50) MORPHY98 a program written by P. L. A. Popelier with a contribution from R. G. A. Bone, UMIST, Manchester England, EU 1998.

(51) Noury, S.; Krokidis, X.; Fuster, F.; Silvi, B., TopMoD package, Université Pierre et Marie Curie, 1997.

(52) Woodward, R. B.; Hoffmann, R. *The Conservation of Orbital Symmetry*; Academic Press: New York, 1970.

Scheme 2. Isodesmic Reaction Paths for the Saturated and Unsaturated Heterocycles[a]

isodesmic reaction (i)

	X			
a	N	**1a**	**7a**	ΔH = 22.8(23.1)
b	P	**1b**	**7b**	8.6(9.5)
c	As	**1c**	**7c**	-1.8(-1.8)

isodesmic reaction (ii)

4a	**8a**	ΔH = 12.8(13.6)
4b	**8b**	-0.8(-0.4)
4c	**8c**	-8.0(-7.8)

isodesmic reaction (iii)

1a	**4a**	ΔH = -5.1(-3.2)
1b	**4b**	17.3(17.9)
1c	**4c**	14.9(14.5)

[a] Values at the B3LYP/6-311G* and in parentheses at the G2 level (all in kcal·mol^{-1}).

exothermic ($\Delta H = -8.0$ kcal·mol^{-1}); however, for the unsaturated reaction i this value was only −1.8 kcal·mol^{-1}, yielding a net stabilization of 6.2 kcal·mol^{-1} for the unsaturated As-oxide compound. This stabilization increased for P- and N-oxides to ca. 10 kcal·mol^{-1}, with the saturated paths (ii): exothermic, isoenergetic and endothermic for As, P, and N, respectively. These considerations have been corroborated at the G2 level, giving similar results (see Scheme 2). The isodesmic reaction iii is another alternative to assess the aromaticity for these rings. This pattern has been used to calculate the resonance energy of the cyclopropenylium ion.[53] The values found in the isodesmic reaction iii yielded a net aromatic stabilization for **1b** and **1c**. However, **1a** was unstable due to the higher N electronegativity (17.9, 14.5, and −3.2 kcal·mol^{-1}, at the G2 level for **1b**, **1c**, and **1a**, respectively).

Geometrical and electronic characterizations have also been made for the structures of Schemes 1 and 2. The numerical results are presented in Tables 1−3 (and Table 4 in the Supporting Information). Table 1 summarizes the geometrical parameters. The phosphirene (**7b**) geometry showed a short double bond in comparison with its oxide **1b** (1.292 and 1.336 Å, respectively). In addition, the P−C bond in **7b** is longer than in **1b** (1.854 vs. 1.761 Å, respectively), compatible with the a delocalization of a double bond in the ring. In addition, the geometrical ring parameters for **1b** were very similar to the aromatic

Table 1. Geometrical Parameters (Å and Deg) for the Structures Studied at the B3LYP/6-311G* Level

	C−C	C−X	X−O	X−H	O−H	∠HXO
H_2C_2NHO, **1a**	1.288	1.508	1.298	1.025		116.8
$H_2C_2N(HO)$, **2a**	1.292	1.460	1.442	1.129	1.347	61.8
H_2C_2NOH, **3a**	1.280	1.467	1.498		0.964	101.5
H_4C_2NHO, **4a**	1.494	1.504	1.314	1.027		116.7
$H_4C_2N(HO)$, **5a**	1.505	1.453	1.471	1.117	1.319	60.2
H_4C_2NOH, **6a**	1.480	1.470	1.447		0.964	101.9
H_2C_2NH, **7a**	1.272	1.523		1.029		
H_4C_2NH, **8a**	1.484	1.472		1.017		
H_2C_2PHO, **1b**	1.336	1.761	1.486	1.409		113.7
$H_2C_2P(HO)$, **2b**	1.332	1.779	1.569	1.499	1.482	57.7
H_2C_2POH, **3b**	1.312	1.800	1.687		0.964	111.3
H_4C_2PHO, **4b**	1.570	1.796	1.491	1.411		117.4
$H_4C_2P(HO)$, **5b**	1.550	1.819	1.583	1.479	1.504	58.7
H_4C_2POH, **6b**	1.504	1.845	1.692		0.960	110.9
H_2C_2PH, **7b**	1.292	1.854		1.444		
H_4C_2PH, **8b**	1.490	1.880		1.420		
H_2C_2AsHO, **1c**	1.330	1.906	1.641	1.517		116.6
$H_2C_2As(HO)$, **2c**	1.329	1.952	1.714	1.573	1.676	61.1
H_2C_2AsOH, **3c**	1.304	1.940	1.844		0.964	109.4
H_4C_2AsHO, **4c**	1.550	1.939	1.646	1.517		119.2
$H_4C_2As(HO)$, **5c**	1.539	1.967	1.726	1.556	1.700	62.2
H_4C_2AsOH, **6c**	1.488	1.991	1.847		0.964	108.8
H_2C_2AsH, **7c**	1.289	1.991		1.552		
H_4C_2AsH, **8c**	1.476	2.023		1.536		

phosphirenylium cation.[24] However, a similar behavior is found comparing phosphirane (**8b**) with phosphirane oxide (**4b**). The data for the corresponding arsenic compounds (**1c**, **4c**, **7c**, and **8c**) followed similar trends.

As previously observed, the situation differs for the nitrogen compounds; comparing aziridine (**8a**) with 1*H*-azirine (**7a**) geometries, we find a large deformation in

(53) with a value of 59.0 kcal·mol^{-1} at the G2 level, see Glukhoutsev, M. N.; Laiter, S.; Pross, A. *J. Phys. Chem.* **1996**, *100*, 17801.

Table 2. Electronic Charge Density, $\rho(r)$ (e/a_o^3), and Its Laplacian, $\nabla^2\rho(r)$ (e/a_o^5), for the Different BCPs for the Nitrogen and Phosphorus Derivatives

bond	$\rho(r)$	$\nabla^2\rho(r)$	$\rho(r)$	$\nabla^2\rho(r)$	$\rho(r)$	$\nabla^2\rho(r)$	$\rho(r)$	$\nabla^2\rho(r)$	$\rho(r)$	$\nabla^2\rho(r)$	$\rho(r)$	$\nabla^2\rho(r)$	$\rho(r)$	$\nabla^2\rho(r)$	ρ(r)	$\nabla^2\rho(r)$
	H_2C_2NHO **1a**		$H_2C_2N(HO)$ **2a**		H_2C_2NOH **3a**		H_4C_2NHO **4a**		$H_4C_2N(HO)$ **5a**		H_4C_2NOH **6a**		H_2C_2NH **7a**		H_4C_2NH **8a**	
N−C	0.236	−0.246	0.256	−0.337	0.261	−0.354	0.238	−0.403	0.257	−0.511	0.257	−0.501	0.234	−0.300	0.255	−0.594
N−O	0.408	−0.494	0.291	−0.114	0.248	−0.091	0.389	−0.397	0.265	−0.019	0.282	−0.253				
C−C	0.356	−1.010	0.353	−0.981	0.355	−0.971	0.244	−0.497	0.237	−0.438	0.242	−0.462	0.366	−1.090	0.252	−0.583
N−H	0.335	−1.581	0.213	−0.571	0.361	−2.341	0.332	−1.534	0.222	−0.651	0.364	−2.418	0.336	−1.526	0.339	−1.623
rcp[a]	0.212	0.398	0.229	0.413	0.235	0.366	0.191	0.257	0.201	0.247	0.204	0.225	0.215	0.282	0.209	0.167
	H_2C_2PHO **1b**		$H_2C_2P(HO)$ **2b**		H_2C_2POH **3b**		H_4C_2PHO **4b**		$H_4C_2P(HO)$ **5b**		H_4C_2POH **6b**		H_2C_2PH **7b**		H_4C_2PH **8b**	
P−C	0.160	0.022	0.153	−0.024	0.148	−0.056	0.163	−0.136	0.155	−0.207	0.148	−0.214	0.135	−0.043	0.137	−0.124
P−O	0.228	1.395	0.194	0.919	0.149	0.382	0.224	1.346	0.189	0.805	0.148	0.385				
C−C	0.334	−0.893	0.336	−0.906	0.347	−0.957	0.215	−0.358	0.224	−0.399	0.241	−0.475	0.364	−1.110	0.260	−0.649
P−H	0.173	−0.264	0.126	−0.182	0.356	−2.311	0.171	−0.258	0.131	−0.213	0.358	−2.348	0.157	−0.138	0.158	−0.082
rcp[a]	0.144	0.154	0.138	0.158	0.137	0.114	0.139	0.032	0.133	0.024	0.132	−0.009	0.123	0.167	0.124	0.018
	H_2C_2AsHO **1c**		$H_2C_2As(HO)$ **2c**		H_2C_2AsOH **3c**		H_4C_2AsHO **4c**		$H_4C_2As(HO)$ **5c**		H_4C_2AsOH **6c**		H_2C_2AsH **7c**		H_4C_2AsH **8c**	
As−C	0.134	0.042	0.128	0.058	0.124	0.064	0.133	−0.025	0.125	−0.006	0.119	0.008	0.113	0.051	0.112	0.004
As−O	0.206	0.584	0.177	0.475	0.130	0.280	0.204	0.553	0.173	0.415	0.129	0.275				
C−C	0.341	−0.952	0.341	−0.953	0.353	−1.005	0.226	−0.431	0.232	−0.458	0.252	−0.543	0.369	−1.143	0.270	−0.706
As−H	0.146	−0.150	0.117	−0.094	0.356	−2.256	0.146	−0.144	0.121	−0.104	0.358	−2.293	0.135	−0.091	0.137	−0.087
rcp[a]	0.120	0.243	0.115	0.248	0.115	0.217	0.113	0.171	0.107	0.175	0.107	0.146	0.105	0.193	0.102	0.135

[a] Ring critical point.

Table 3. Calculated[a] NMR δ_C and δ_H Chemical Shifts (ppm)[a] Together with the Isotropic Values for O and X (N, As, or P)

	δ_C	δ_H [b]	δ_N	δ_O		δ_C	δ_H [b]	δ_P	δ_O		δ_C	δ_H [b]	δ_{As}	δ_O
H_2C_2NHO, **1a**	134.4	5.9	189.1	164.2	H_2C_2PHO **1b**	164.6	6.9	481.9	275.9	H_2C_2AsHO **1c**	164.7	6.8	1679.8	264.2
$H_2C_2N(HO)$, **2a**	125.5	21.9	225.7	53.2	$H_2C_2P(HO)$ **2b**	172.5	20.6	426.5	61.9	$H_2C_2As(HO)$ **2c**	174.2	20.3	1554.5	3.9
H_2C_2NOH, **3a**	123.1	3.0	151.3	162.7	H_2C_2POH **3b**	143.5	1.0	485.8	273.0	H_2C_2AsOH **3c**	142.4	−0.2	1811.0	303.1
H_4C_2NHO, **4a**	33.3	4.2	185.7	178.0	H_4C_2PHO **4b**	1.8	6.1	452.6	353.6	H_4C_2AsHO **4c**	4.4	5.7	1668.4	361.1
$H_4C_2N(HO)$, **5a**	27.7	18.3	248.0	8.9	$H_4C_2P(HO)$ **5b**	8.8	22.1	390.2	227.9	$H_4C_2As(OH)$ **5c**	16.5	20.1	1573.0	276.9
H_4C_2NOH, **6a**	27.0	3.2	170.4	209.2	H_4C_2POH **6b**	5.3	−0.1	465.7	343.3	H_4C_2AsOH **6c**	15.1	−1.5	1774.5	377.2
H_2C_2NH, **7a**	117.5	−0.6	270.6		H_2C_2PH **7b**	121.3	2.3	639.4		H_2C_2AsH **7c**	121.2	2.2	2188.0	
H_4C_2NH, **8a**	15.2	−1.0	274.3		H_4C_2PH **8b**	−0.6	−0.3	692.4		H_4C_2AsH **8c**	8.6	−0.1	2300.2	

[a] Tetramethylsilane signal as reference for the δ_C and δ_H shifts. [b] Hydrogen bonded to X or O atom.

the 1*H*-azirine geometry, with the C−N lengthening (1.523 Å) in comparison with the C−N bond in aziridine (**8a**) (1.472 Å). However, the double bond in 1*H*-azirine shows a standard value (1.272 Å). On the other hand, comparing **8a** with the *N*-oxide (**4a**), a lengthening is observed for the C−N bond in **4a** as opposed to the P derivatives. Nevertheless, a net stabilization of ca. 13 kcal·mol^{-1} results, according to the isodesmic reaction ii shown in Scheme 2. This stabilization is explained by a σ^* C−N bond negative hyperconjugation[3] in the N−O bond formation on **4a**, yielding N−O bond distances shorter than for trimethylamine *N*-oxides[13,54] (1.314 vs 1.365 Å, respectively). The additional C═C in 1*H*-azirine *N*-oxide (**1a**) gave an additional stabilization (see Scheme 2). The C−N bonds shortened from 1.523 to 1.508 Å for **7a** and **1a**, respectively, with a minor lengthening of the corresponding C═C. Therefore, the C−N bond in **1a** is larger than **8a**. The above considerations explain the different behavior of the N-derivatives compared with the P or As ones.

The geometrical trends, shown by **1a**−**c** and **4a**−**c**, in comparison with the heterocycles **7a**−**c** and **8a**−**c**, have also been supported by their electronic properties, (Tables 2−4). Table 2 lists the numerical parameters of the different BCPs in the $\rho(r)$; Table 3 shows the theoretical nuclear magnetic resonance (NMR) chemical shifts (δ); and Table 4 gives the electronic population of the different basins of ELF (Supporting Information).

The P- and As-oxides have shown similar trends, also in their electronic properties. The C−X BCPs $\rho(r)$ values for **1b** and **1c** were larger than their parent heterocycles (**7b** and **7c**). In addition, the corresponding C═C BCP values were smaller (0.135 and 0.113 e/a_o^3 for C−X bond and 0.354 and 0.369 e/a_o^3 for C═C for **7b** and **7c**, respectively vs. 0.160 and 0.134 for C−X and 0.334, 0.341 for C═C for **1b** and **1c**, respectively, see Tables 2 and 4). Also, the ellipticity, ϵ, values decreased for the C═C in **1b** (0.185) and **1c** (0.229) compared to **7b** (0.285) and **7c** (0.287), whereas $\rho(r)$ for all the ring BCP remained high. This is compatible with an electronic charge concentration above and below the ring plane. A parallel trend in the electronic charge concentration, $-\nabla^2\rho(r)$, appeared in **1b** and **1c** compared with **7b** and **7c**. Furthermore, the RCP for **1b** and **1c** had higher $\rho(r)$ values than for **7b** and **7c**. All these data agree with a high electron density delocalization in the ring. However, similar behavior appeared in the saturated oxides (**4b** and **4c**), compared with **8b** and **8c**.

Although the ELF and $-\nabla^2\rho(r)$ fields have a general homomorphism,[55] additional information on the bonding properties can be gained from ELF topological analysis. This analysis has been performed, and the results are presented in Table 4 (Supporting Information). The electron population[56] on the different basins has been calculated by integration of $\rho(r)$ over the basins for **1a**−**c** to **8a**−**c**, together with the standard deviation, relative fluctuation and contribution analysis of the other basins. For **8b** with a standard C−C single bond, a V(C,C) basin population of ca. 2 electrons was found, with smaller V(P,C) values (ca. 1.6 e$^-$). However, the relative fluctua-

(54) Dobado, J. A.; Martínez-García, H.; Molina, J.; Sundberg M. R. *J. Am. Chem. Soc.* **1999**, *121*, 3151.

(55) Bader, R. F. W.; Johnson, S.; Tang, T. H.; Popelier, P. L. A. *J. Phys. Chem.* **1996**, *100*, 15398.

tion for this latter basin proved higher than in the former one. The contribution analysis for the *V*(C,C) basin was ca. 15% for each *V*(C,H) and ca. 13% for each *V*(P,C) basin, the *V*(P,C2) contribution being ca. 16% for each *V*(C2,H), ca. 11% for the *V*(P,H), 9% for the other *V*(P,C3), 14% for the *V*(C,C) and 20% for the *V*(P) basins. The standard C=C bond of **7b** presented two *V*(C,C) basins. The main contribution for one of the *V*(C,C) basins came from the other one (26%), with the remaining contributions almost unchanged (see Table 4, Supporting Information). The situation is quite similar, in the saturated oxide (**4b**), compared to the parent heterocycle (**8b**). In addition, two new *V*(P,O) and *V*(O) basins appeared, with small contributions from the *V*(P,C) basins (<8%); these were compatible with a small contribution from negative hyperconjugation.

In structure **1b** with C=C and P−O groups, the situation changed noticeably, with only one *V*(C,C) basin of low population (3.00 vs 3.46 e^-, for **7b**). The V(P,C) population increased in comparison with **4b** (2.26 vs 1.95 e^-, respectively). All these data agree with a net electron delocalization in the ring, corroborated also by the contribution analysis of the valence basin of **1b**. Thus, the main *V*(P,C2) and *V*(P,C3) contributions to *V*(C,C) were ca. 22% (ca. 14% for **4b**, **7b**, and **8b**, respectively). The *V*(P,C2) or *V*(P,C3) contribution analysis from *V*(C,C) was also large (27%). In addition, the *V*(P,O) contribution showed low values from the *V*(C,C) and *V*(P,C) basins (<7%), also in agreement with a very small negative hyperconjugation. The data for the arsenic derivatives (**1c**, **4c**, **7c**, and **8c**) had similar trends, with a net electron delocalization in **1c** ring (see Table 4, Supporting Information).

The different trend of the N-derivatives is also corroborated in Table 4 (Supporting Information), with a small variation in the V(N,C) population, comparing the saturated *N*-oxide (**4a**) with **1a** (1.81 vs 1.88 e^-, respectively). In addition, there was also a very small variation for *V*(C,C) in **7a** compared to **1a** (3.70 vs. 3.72 e^-, respectively). Consequently, there was no additional electron delocalization in the oxide formation for the unsaturated compounds.

Moreover, there were larger *V*(N,O) contributions from the *V*(N,C) basins, due to a negative hyperconjugation in the N−O bond formation.

This different behavior of the nitrogen compounds is also addressed by the calculated NMR δ_C and δ_H chemical shifts (see Table 3). The unsaturated heterocyles **7a**−**c** had standard olefinic carbons for **7a**−**c** (ca. 120 ppm). The saturated heterocycles (**8a**−**c**) presented standard δ_C values (ca. 15, 0, and 8 ppm for **8a**, **8b**, and **8c**, respectively). A moderate δ_C downfield shift was observed for **4a** (with a N−O bond) in comparison with **8a** (33 vs 15 ppm, respectively). A similar shift was also observed for **1a** vs **7a** (134 vs 117 ppm, respectively). However, a different behavior was displayed for P and As derivatives; there was a small δ_C variation passing from **8b** and **8c** to the oxides **4b** and **4c** (<4 ppm). Moreover, a large variation was found from **7b** and **7c** to the unsaturated oxides **1b** and **1c** (>43 ppm), with an olefinic δ_C ca. 164 ppm. In addition, the δ_H values also appeared at lowfield (ca. 9 ppm), supporting the ideas of a high electron delocalization for **1b** and **1c**.

Scheme 1 displays the MR path, for the saturated and unsaturated oxides **1a**−**c** and **4a**−**c**, with smaller activation energies ($\Delta H^{\ddagger}$) for N compounds than for P and As ones (36−38, 57−61, and 43−46 kcal·mol^{-1}, respectively). This rearrangement is analyzed by means of the geometries and electronic properties of the oxides, TSs and hydroxyl derivatives (products).

The geometrical changes for the path oxides → [TSs] → hydroxide derivatives are analogous for the P and As series, being different for the N ones. The C=C bond slightly decreased from **1b** → **2b** → **3b** (1.336, 1.332, and 1.312 Å, respectively), with a slight C−P lengthening (1.761, 1.779, and 1.800 Å, respectively). In general, the overall ring geometries for **2b** were very close to **1b**, the main geometrical differences appearing in the P−O bond (1.486, 1.569, and 1.687 Å, respectively). These geometrical trends are very similar for the saturated derivatives **4b**, **5b** and **6b**. In addition, the large C−C bond in **4b** (1.57 Å) compared to the phosphirane heterocycle is noteworthy (see Table 1). This lengthening is accompanied by a shortening in the P−C bond. The As derivatives showed similar trends, yielding TSs (**2c** and **5c**) with geometrical parameters similar to the parent oxides.

The nitrogen series gave different geometrical behavior, with unchanged C=C bond (1.288, 1.292 and 1.280 Å for **1a**, **2a**, and **3a**, respectively). Moreover, similar trends were observed for the saturated path (1.494, 1.505, and 1.480 Å for **4a**, **5a**, and **6a**, respectively). The C−N bond shortened from **1a** or **4a** to the corresponding TSs (ca. 1.51 to 1.46 Å, respectively) and remained almost unchanged from the TSs to the hydroxyl derivatives **3a** and **6a** (see Table 1). The N−O bond followed the same trend with large variation from oxides to the TSs, and very small variation from the TSs to the hydroxyl derivatives (1.298, 1.442, and 1.498 Å for **1a**, **2a**, and **3a**, respectively). This trend was also observed for the saturated nitrogen derivatives, and, moreover, both TSs (**2a** and **5a**) showed similar geometrical behavior than the products (**3a** and **6a**).

The geometrical trends for the P and As derivatives were confirmed by the ρ(r) and ELF analyses. Thus, the C−C and C−P $\rho(r)$ values at the BCP remained almost unchanged for the oxides and TSs, the main differences appearing in the P−O BCPs with values of 0.228 and 0.194 e/a_o^3 for **1b** and **2b**, respectively. The rearrangement for the N derivatives had a different behavior, with the $\rho(r)$ values for the C=C bond remaining almost unchanged (ca. 0.35 e/a_o^3 for **1a** and **2a**). However, the $\rho(r)$ and $-\nabla^2\rho(r)$ values increased noticeably for the C−N BCP passing from the reactives to the TSs (0.236 e/a_o^3, −0.246 e/a_o^5, and 0.256 e/a_o^3, −0.337 e/a_o^5 for **1a** and **2a**, respectively) in agreement with a bond shortening. These values were very similar for the products and TSs. The general trends were also observed for the saturated compounds, in agreement with the nonparticipation of the negative hyperconjugation for the N−O bond in the

(56) Considering the scalar character of the ELF function, the analysis of their gradient fields yields their attractors (local maxima) and their corresponding basins. There are two type of basins: the core basins labeled by C(atom symbol) and the valence basins V(list of atoms). The valence basins are characterized by their synaptic order (the number of core basins with which they share a common boundary). Accordingly, they can be classified as mono, di and polysynaptic, corresponding to the lone pair, bicentric and polycentric bonding region, respectively. The quantitative population on the different basins are obtained by integrating a given density of property over the volume of the basins. The following definitions are used through the text: basin population $\bar{N}(\Omega_i) = \int_{\Omega_i}\rho(r)dr$ and its variance $\sigma^2(\Omega_i) = \int_{\Omega_i}\int_{\Omega_i}\pi(r,r')drdr' + \bar{N}(\Omega_i) - \bar{N}^2(\Omega_i)$ in which $\pi(r,r')$ is the two electron density, and the relative fluctuation $\lambda(\Omega_i) = \sigma^2(\Omega_i)/\bar{N}(\Omega_i)$.

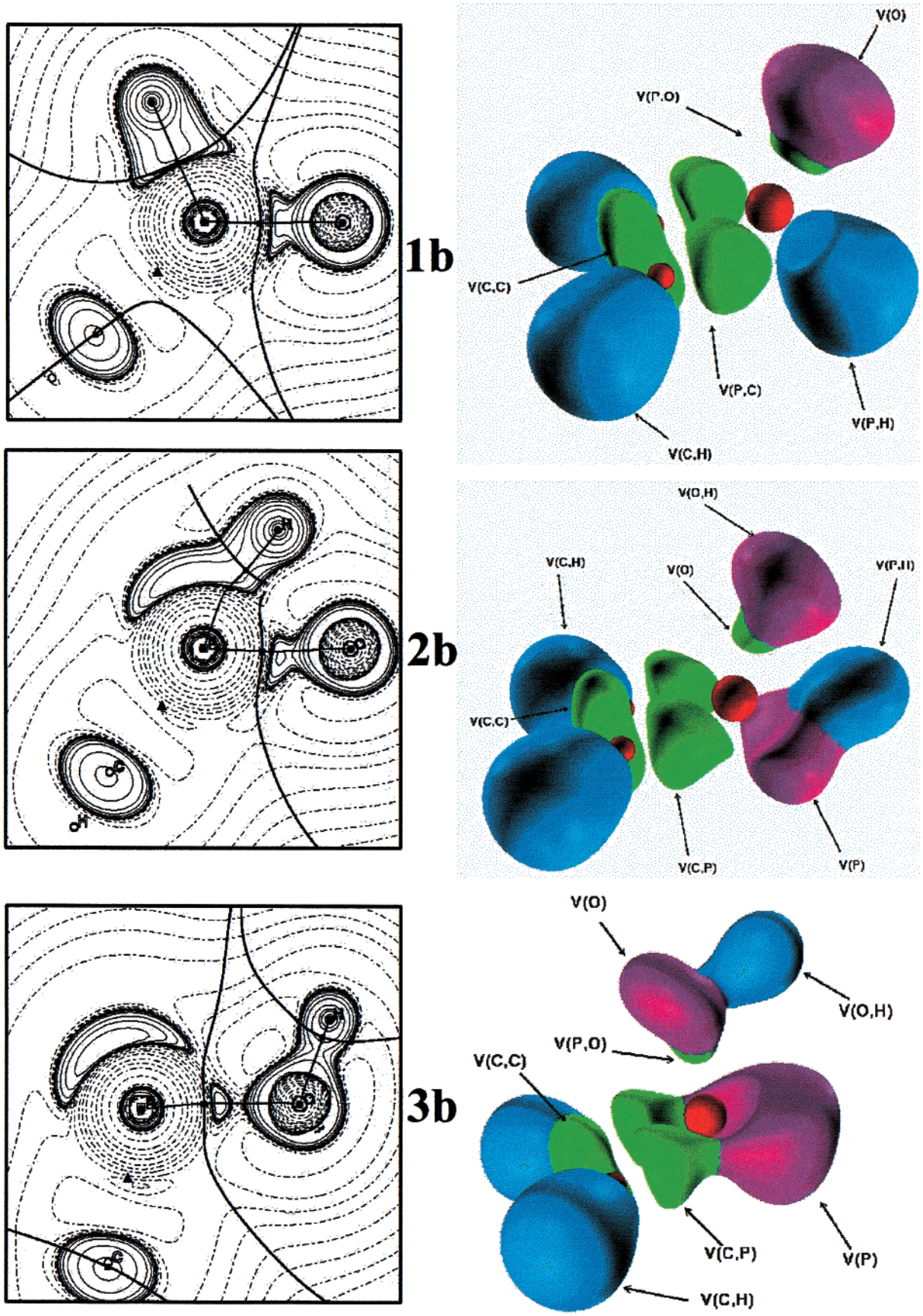

Figure 1. (i) $\nabla^2\rho(r)$ contour maps on the symmetry plane, obtained using the MORPHY98 program,[50] for structures **1b**, **2b**, and **3b**. The contours begin at zero and they increase (solid contours) and decrease (dashed contours) in steps of ±0.02, ±0.04, ±0.08, ±0.2, ±0.4, ±0.8, ±2.0, ±4.0, ±8.0. The thick solid lines represent the molecular graph that joins the nuclei (solid circles) and the BCP (solid squares), and also represent the zero flux surface. **(**ii) Electron localization function (ELF) isosurface plot (0.78) for structures **1b**, **2b**, and **3b**, at B3LYP/6-311G* theoretical level.

TSs. The N−O BCP $\rho(r)$ values also showed this behavior (0.408, 0.291, and 0.248 e/a_o^3 for **1a**, **2a**, and **3a**, respectively).

The valence basins V(C,C) and V(X,C) populations (X = P and As) remained almost unchanged through the path (ca. **3.0** in V(C,C) and ca. **2.2** e^- in V(P,C), for **1b**, **2b**, and **3b**). In addition, the changes in the basin population values passing from the TS to the product (**2b** → **3b**) were also small. In general, the trends for the **1b** → **3b** path were also followed by the As and the saturated P derivatives (see Table 2). Moreover, a remarkable behavior appeared in the V(N,C) population variation across the path. This population was larger for the reactives (**1a** and **4a**) than for the TSs (**2a** and **5a**), and even larger than for the products (**3a** and **6a**). A reasonable explanation for this apparent contradictory trend was the presence of negative hyperconjugation for **1a** or **4a** (yielding electron delocalization for the V(O) in the C−N bond) together with the C−N shortening in the TSs (absence of negative hyperconjugation and σ^* C−N population, decreasing the population).

The aforementioned trends were contradictory with the shortening of the C−N bond in the path (**1a** → **2a** or **4a** → **5a**). The absence of negative hyperconjugation for the TSs lengthened the N−O bond.

The ELF and $\nabla^2\rho(r)$ topological analyses gave a clear picture of the reaction. That is, in the reactives, there were no monosynaptic V(X,H) valence basins, and, for the N TSs, larger electron populations appeared than for the P ones. On the other hand, the population of the disynaptic V(X,H) basin decreased in the TSs with respect to the reactives, also yielding smaller populations on the N basin than in the P ones. These V(X,H) basins disappeared for the products, the population of the monosynaptic V(X) basin corresponded to the X lone pair, and a new disynaptic V(O,H) appeared for the products (see Figure 1).

The different behavior of the N rearrangement was also supported by the calculated chemical shifts. Thus, the δ_C shifts for **2b** and **2c** were similar to those of **1b** and **1c** (ca. 170 ppm). Furthermore, a larger ring electron delocalization was also observed for the TSs, compatible with larger δ_H values (ca. 10 for **2b** vs ca. 9 ppm for **1b**). However, this electron delocalization decreased on the corresponding products, yielding δ_H and δ_C shifts closer to the double bond in the unsaturated parent heterocycles. The N derivatives presented a different behavior, with δ_C values similar for **2a** and **3a**, showing analogous trend for the δ_H values, compatible with a TS resembling the products.

IV. Conclusions

The geometrical and electronic properties of the proposed oxides have been characterized, using the AIM and ELF topologies together with the calculated chemical shifts. An electronic delocalization, characteristic of aromatic structures, was found only for the unsaturated phosphorus and arsenic oxide derivatives. Thus, the nonaromaticity of the amine oxide derivatives was explained by negative hyperconjugative effects in the N−O bond formation, and the similar electronegativity of the N compared to O.

Theoretical study of MR, by a proton migration to the oxygen atom, has been made for the saturated and unsaturated strained cyclic amine, phosphine and arsine oxides. All the reactions became exothermic but with high $\Delta H^{\ddagger}$ values. The presence of a C=C double bond in the structures does not appreciably change the reaction energetic profile. However, the nitrogen derivatives presented the lowest $\Delta H^{\ddagger}$ values. Preliminary calculations on a radical dissociation-recombination path for the MR yielded higher energetic profiles (>25 kcal·mol^{-1}) than did the proton-migration mechanism, and consequently it has been discarded.

To test the C=C influence in the structures, we performed isodesmic reactions, giving a net stabilization for the unsaturated oxides vs the saturated ones (ca. 10 kcal·mol^{-1} at the B3LYP/6-311G* level), corroborated at higher theoretical levels (G2 method). In addition, aromatic stabilization has been achieved for **1b** and **1c** (17.9 and 14.5 kcal·mol^{-1} at the G2 level).

The MR mechanism has been characterized by the study of the geometrical and electronic properties of the reactives, TSs and products. The behavior of the P and As derivatives also showed a similar trend and different to that of the N ones. In the first case (P and As) the TSs were closer to the reactives. However, the N derivative reactions displayed TS structures closer to the products.

Acknowledgment. Computing time was provided by the Universidad de Granada (Spain). We are grateful to Professor R. F. W. Bader for a copy of the AIMPAC package of programs. We thank Professor B. Silvi for a copy of TopMoD package of program. We also thank D. Nesbitt for reviewing the language of the English manuscript.

Supporting Information Available: Table 4 with the electronic population of the different basins of ELF. This material is available free of charge via the Internet at http://pubs.acs.org.

JO0056040